sustainability

MDPI

Article

A Novel Polygeneration System Based on a Solar-Assisted Desiccant Cooling System for Residential Buildings: An Energy and Environmental Analysis

Luis Gabriel Gesteira * and Javier Uche

CIRCE Research Institute, University of Zaragoza, 50018 Zaragoza, Spain; javiuche@unizar.es
* Correspondence: 773948@unizar.es

Abstract: This work aims to design and dynamically simulate a polygeneration system that integrates a solar-assisted desiccant cooling system for residential applications as an alternative to vapor compression systems. The overall plant layout supplies electricity, space heating and cooling, domestic hot water, and freshwater for a single-family townhouse located in the city of Almería in Spain. The leading technologies used in the system are photovoltaic/thermal collectors, reverse osmosis, and desiccant air conditioning. The system model was developed and accurately simulated in the TRNSYS environment for a 1-year simulation with a 5-min time step. Design optimization was carried out to investigate the system's best configuration. The optimal structure showed a satisfactory total annual energy efficiency in solar collectors of about 0.35 and about 0.47 for desiccant air conditioning. Coverage of electricity, space heating and cooling, domestic hot water, and freshwater was 104.1%, 87.01%, 97.98%, 96.05 %, and 100 %, respectively. Furthermore, significant ratios for primary energy saving, 98.62%, and CO_2 saving, 97.17%, were achieved. The users' thermal comfort level was satisfactory over the entire year. Finally, a comparison with an alternative coastal site was performed to extend the polygeneration system's applicability.

Keywords: residential sector; renewable energy; polygeneration system; desiccant air conditioning; TRNSYS; sustainability

Citation: Gesteira, L.G.; Uche, J. A Novel Polygeneration System Based on a Solar-Assisted Desiccant Cooling System for Residential Buildings: An Energy and Environmental Analysis. *Sustainability* **2022**, *14*, 3449. https://doi.org/10.3390/su14063449

Academic Editors: Francesco Liberato Cappiello, Francesco Calise and Maria Vicidomini

Received: 22 February 2022
Accepted: 14 March 2022
Published: 15 March 2022

1. Introduction

In the past half century, population growth and economic development improved awareness about the environmental burdens of conventional energy systems. It directed the research community and governments' attention to alternative energy sources to cope with the increasing energy demand, global climate change, and high levels of greenhouse gas emissions. In recent years, the International Energy Agency (IEA) [1] and the European Union (EU) [2] focused on energy consumption, particularly related to buildings. In 2016, the European Commission developed guidelines for promoting nearly zero-energy buildings (NZEBs) [3], as the building sector is responsible for about 40% of global energy consumption and more than 30% of greenhouse gas emissions [4]. Furthermore, around 75% of buildings are energy inefficient, and 80% of their energy efficiency potential remains an opportunity to explore economic gains, energy security improvements, and environmental protection [5].

In this framework, the application of polygeneration systems within buildings presents an exciting alternative for energy consumption reduction and, consequently, the accomplishment of the NZEBs target [6]. Several research works are available in the literature studying polygeneration systems integrated into diverse building types such as hotels [7], hospitals [8], residences [9], districts [10], offices [11], schools [12], etc., and evaluating the systems' performance with dynamic simulation tools that take into account the buildings' main demands.

Polygeneration systems can achieve more than 80% of energy savings with an appropriate level of energy integration, especially in warm areas such as the European Mediterranean countries [13]. It can replace conventional technologies based on fossil fuels and simultaneously produce several energy services by significantly reducing primary energy consumption and CO_2 emissions. The configuration of polygeneration systems can also vary widely to be suitable for different applications. Input energy may be renewable or non-renewable, while outputs are mainly electricity, heating, cooling, chemicals, liquid or gaseous fuels, and potable water. According to its performance goals, assessments are based on three indicators, i.e., technical, economic, and environmental [14].

Many researchers have evaluated such polygeneration systems using a broad assortment of superstructures and assessment procedures. A polygeneration scheme providing power, heat, and water for a single dwelling was studied in-depth by the authors some years ago. Acevedo et al. [15] designed a system combining photovoltaic/thermal collectors, an evacuated tube collector, and a wind turbine. The system also included two desalination technologies and two types of energy storage devices. Coverage of hot water, freshwater, and power was 99.3%, 100%, and 70%, respectively. Uche et al. [16] reported an experimental study of the same polygeneration system. Those tests showed that daytime assessments of power, freshwater, and sanitary hot water allowed for excellent coverage of scheduled energy and water demands. Flexible operation due to the combined production of power and heat was also observed. An environmental assessment of the pilot unit and its life cycle showed low impacts concerning the conventional supply of energy and water. Finally, Usón et al. [17] investigated the exergy and exergy cost of the previous polygeneration system. The system showed an exergy efficiency of 7.76% in the base case.

Currently, the most deployed cooling technologies in polygeneration systems are vapor compression (VC) systems and absorption (AB) and adsorption (AD) chillers. Besides its high COP, VC systems use harmful refrigerants with global warming and/or ozone depletion potential. Thus, it is not a sustainable option. AB and AD chillers are large and complex, constraining their use in domestic building applications [18]. An alternative cooling technology for small-scale units is desiccant air conditioning (DAC), demonstrating several advantages in operation life, maintenance, and efficiency [18]. A desiccant cooling system uses the capability of desiccant materials to remove moisture from an air stream by a natural adsorption process. Thus, it can achieve thermal comfort for buildings since it can control the sensible and latent loads separately and, consequently, improve the Indoor Air Quality (IAQ) [19].

The recent literature shows a significant research effort regarding various desiccant cooling system configurations. Jani et al. [20] simulated a system with a hybrid desiccant wheel using different configurations for hot and humid climatic conditions. Experimental measurements also observed the influence of operating parameters on system performance. Simulated results were validated as being a good match with the experimentally measured data. Elgendy et al. [21] performed a simulation study on desiccant air conditioning with direct and indirect evaporative coolers using TRNSYS [22]. The study found that desiccant cooling systems with an indirect evaporative cooler have a higher COP. Angrisani et al. [23] examined the desiccant cooling system with three different configurations for the climatic conditions of Italy and compared the performance with the conventional air conditioning system. It was found that 20–25% of primary energy savings can be achieved while CO_2 emissions can also be reduced up to 35–40%. Sopian et al. [24] investigated the desiccant cooling system with one and two stages and in ventilation and recirculation configurations, performed in the TRNSYS [22] simulation studio for Malaysia's hot and humid weather conditions. The two-stage ventilation mode was the best among the other arrangements, presenting a COP of up to 1.06.

Thermal energy sources at low and medium temperatures, typically within 50–80 °C, and obtainable by solar collectors are often used as inputs in DAC applications [25]. Thus, a solar-assisted desiccant cooling system can promote environmental pollution reduction and energy consumption savings. Furthermore, it can also significantly contribute to

the implementation of NZEBs [26]. In particular, Farooq et al. [27] studied dynamic simulation and performance parameters for three ventilation schemes of a DAC based on a photovoltaic-thermal solar collector for the weather of Lahore in Pakistan. The primary energy savings, solar fraction, and thermal efficiency of the solar collector were used to compare its performances. A dynamic analysis of a solar desiccant cooling system was performed by Heidari et al. [28] to produce the cooling effect and freshwater for domestic use. The simulation results showed that the proposed system could provide a comfortable temperature in a hot and humid climate. The system led to an 18.7% saving of CO_2 emissions over a month and economic feasibility, with a payback period of 3 years.

Finally, industrial applications have studied the leading solar cooling technologies integrated into polygeneration schemes for cooling, heating, electricity, and desalinated water production [29]. Thus, it calls for an improvement of existing optimization approaches that considers the synthesis of polygeneration systems supported by renewable energy sources for building applications [30]. Therefore, this study analyses an installation's energy and environmental feasibility in supplying the five demands of a dwelling, as well as its design optimization.

2. Materials and Methods

2.1. System Layout

A simplified layout of the system under investigation in this paper is shown in Figure 1. The proposed system serves a residential building. The technologies included in the system are a photovoltaic/thermal (PVT) collector for electricity and heating, thermal energy storage (TES), reverse osmosis (RO) for freshwater and hot sanitary water demands, and desiccant air conditioning (DAC) for cooling. Additional components were implemented in the system, such as pumps, pipes, heat sinks, etc. The design parameters for all system components were accurately selected to allow the system to operate correctly. In particular, set-point temperatures and dead temperature bands for the components were chosen to minimize the number of on–off events. Pipes simulate the ductwork.

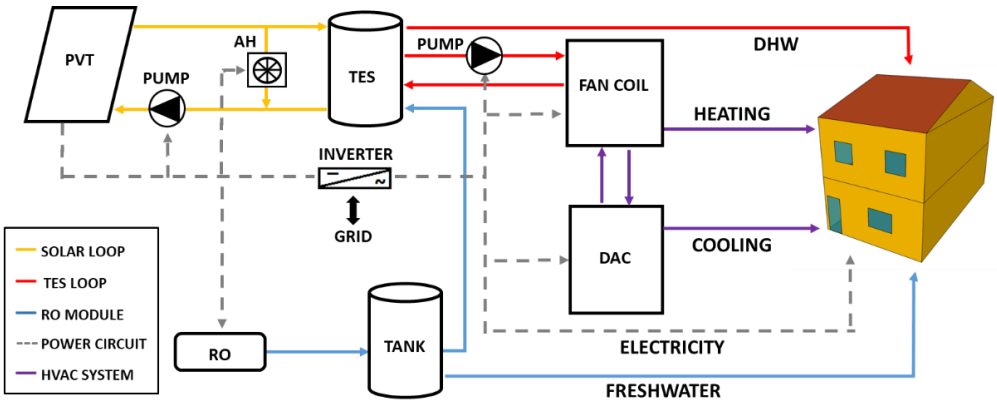

Figure 1. Polygeneration system layout.

The main subsystems included in the system are detailed as follows:

2.1.1. Solar Loop

Solar irradiation is converted into electrical and thermal energy through the PVT collectors. A fixed slope of 35° (no tracking) provides the best irradiation yield for the location of Almería in Spain, according to the Meteonorm weather data simulation. The solar thermal energy produced heats up the solar collector fluid (SCF) circulating through the PVTs. The SCF used in the system is a mixture of water/glycol (60/40). The SCF flow rate of the fixed speed pump is regulated by a controller activated when the PVTs outlet temperature, $T_{out,PVT}$, is 7 °C higher than the temperature at the bottom of the thermal energy storage (TES), $T_{bottom,TES}$, and deactivated when this temperature difference

reaches 2 °C. Thus, the controller stops the pump, preventing the dissipation of the tank's thermal energy.

2.1.2. TES Loop

The thermal energy storage mitigates the fluctuations due to solar radiation variability. It consists of a fluid-filled sensible vertically stratified (4 nodes) energy storage tank with a heat exchanger inside. To avoid the SCF overheating and the PVT electrical efficiency decreasing, a thermostat controls the TES's top temperature with a fixed set point, i.e., $T_{top,TES}$. An air heater (AH) cools the SCF down whenever the PVT's outlet temperature increases the $T_{top,TES}$ over the set point. The heating dissipation capacity of the AH is 20 kW. The TES outputs feed the HVAC system and the DHW simultaneously.

Regarding the DHW, a tempering valve mixes the hot water from the TES with the freshwater from the desalinated water tank. It regulates the outlet temperature for the DHW, $T_{out,DHW}$, equal to 45 °C. The HVAC system provides heating during winter and cooling during summer.

2.1.3. Power Circuit

The electricity system consumption is mostly comprised of the building's electric demand and includes the power loads of pumps, fans, some DAC components, and the RO device. The PVT collector's power is connected to an inverter with peak-power tracking. The inverter converts the DC power from generation to AC and sends it to electric devices. It allows for the purchase and sale of the power back to the utility. When the power produced is higher than the power demand, the surplus power is delivered to the national electric grid. When the energy produced is insufficient to match the power demand, the power is withdrawn from the grid. The grid works as a backup due to the solar collector's intermittent behavior and the non-simultaneity between production and consumption [30].

Furthermore, batteries for these facilities are expensive and require significant maintenance [31]. For simplicity, we assumed an annual near-zero energy balance for the electricity demand. However, as an economic analysis of this study was not performed, a deep discussion on pricing policies was neglected. Detailed analysis on residential sector regulation in Spain is reported by Pinto et al. [32].

2.1.4. RO Module

Membrane-based technology is the most efficient seawater desalination technology due to its comparatively low energy consumption and high salt rejection [33]. Thus, RO seawater desalination was selected to integrate the polygeneration system to provide freshwater. The RO module requires DC power consumption of 110 W, and produces 35 kg/h of freshwater; thus, it presents 3.14 kWh/m^3 of specific consumption [16]. According to its steady performance, the RO module is simulated as a forcing function of power load and freshwater flow instead of a new model type. Thus, it exclusively depends on the electricity, which the grid can attend to, as previously explained. The desalinated water is sent to a tank of 1.0 m^3, and a simple controller prevents overfilling and allows a minimum water capacity of 0.1 m^3.

2.1.5. HVAC System

The TES supplies thermal energy whenever the user requires heating or cooling throughout the year to meet the building HVAC demand. A thermostat inside the thermal building zone controls the setpoint for heating, $T_{set,heat}$, and cooling, $T_{set,cool}$, with a dead band of 2 °C. The seasons of the year activate a single-speed pump to supply hot water for the heating coil or regenerator. In the winter period (from 1 October to 31 May), the thermal energy produced by the PVTs is directly exploited for building space heating through the heating coil. On the other hand, during summer (from 1 June to 30 September), the regenerator uses the PVT's heat energy to drive a DAC system and provide building-space cooling. In addition, the fan airflow calculation is based on the ASHRAE recommendations,

as explained in Ref. [22]. The equation considers the peaks of the heating and cooling demands to calculate the airflow.

2.2. System Model

The proposed system is developed and dynamically simulated in the TRNSYS environment (version 18). It includes several subsystems listed in the previous section. The subsystems are linked to each other to perform the overall system simulation. Some component models are taken from the build-in library of types (e.g., pumps, valves, mixers, diverters, tanks, etc.). Others are user-defined, such as schedulers, controllers, and input data readers. Moreover, the simulation also includes many additional components required to run the simulations and process the results, such as calculators, weather data readers, integrators, and plotters. All main types used in the proposed system model are listed in Table 1.

Table 1. TRNSYS main types used in the proposed system model.

Type	Number	Type	Number
Weather data reader	15	Building	56
Photovoltaic/thermal collector	50	Single-speed fan	146
Inverter	48	Desiccant wheel	716
Fixed flow pump	114	Evaporative coolers	506
Diverter	11	Heat recovery wheel	760
Mixer	11	Heating coil	670
Pipes	31	Thermostats	113, 166
Tanks	39,156	Differential controller	165

In this section, for the sake of brevity, only a detailed description of the PVT collector, the DAC system, and the thermal comfort and energy models are reported. A detailed description of the other component models used in the simulation is omitted; however, it is available in the TRNSYS's component mathematical reference [22]. The technical data concerning the design and operating parameters of the main types are presented in Table 2.

Table 2. Main design and operation parameters.

Type	Parameter	Symbol	Value	Unit
	Solar Loop			
PVT	Slope	θ_S	35	°
	Azimuth	θ_A	0	°
	PVT fin efficiency factor	f_P	0.96	–
	SCF specific heat	c_f	3.89	kJ/kg K
	Collector plate absorptance	α	0.92	–
	Collector plate emittance	ε_p	0.85	–
	Collector loss coefficient	U	16	kJ/h m^2 K
	Transmission-absorption product	$(\tau\alpha)$	0.85	–
	PV efficiency temperature coefficient	β_{PV}	0.0032	1/°C
	PV efficiency reference temperature	T_{ref}	25	°C
	PVT packing factor	P_f	0.8	–
	PV electrical efficiency at Tref	$\eta_{PV,\ ref}$	0.16	–
Air heater	Heat dissipation capacity	Q_{AH}	20	kW
	Effectiveness	ε_{AH}	0.7	–
	Nominal air flow rate	m_{AH}	1716	kg/h
	Power consumption	P_{AH}	0.12	kWh
Pump 1	Nominal flow rate per PVT area	m_f /A_{PVT}	50	kg/h m^2
	Overall efficiency	$\eta_{p,1}$	0.8	–
	Power consumption	$P_{p,1}$	0.025	kWh

Table 2. *Cont.*

Type	Parameter	Symbol	Value	Unit
	TES loop			
TES	TES volume/PVT area	V_{TES}/A_{PVT}	0.1	m^3/m^2
	Number of nodes	n_{TES}	4	–
	Height	h_{TES}	2	m
	Loss coefficient	H	2.5	kJ/h m^2 K
Pump 2	Nominal flow rate	m_w	236	kg/h
	Overall efficiency	$\eta_{p,2}$	0.8	–
	Power consumption	$P_{p,2}$	0.01	kWh
	HVAC system			
DW	F1 Effectiveness	η_{F1}	0.08	–
	F2 Effectiveness	η_{F2}	0.95	–
HRW	Sensible effectiveness	ε_{HRW}	0.8	–
	Power consumption	P_{HRW}	0.18	kWh
DEC	Saturation efficiency	ε_{DEC}	0.85	–
	Power consumption	P_{DEC}	0.08	kWh
HX	Effectiveness	ε_{HX}	0.85	–
Fan	Air flow rate	m_a	963.6	kg/h
	Motor efficiency	η_a	0.84	–
	Power consumption	P_a	0.12	kWh
	RO module			
RO	Power consumption	P_{RO}	0.11	kWh
	Freshwater production	X_{RO}	0.035	m^3/h
	Tank volume	V_{TK}	1.0	m^3
	Power circuit			
Inverter	Efficiency	η_i	0.9	–

2.2.1. PVT Collector Model

The PVT collectors combine photovoltaic panels, PV, and solar thermal collectors, SC, in a unique sheet-and-tube collector with a PV module over the absorber [34]. It consists of a set of components: a glass cover, a PV film encapsulated in the absorber, flow channels, and thermal insulation [35].

The PVT component has eight operational modes in the TRNSYS library, which vary the calculation method for the thermal loss coefficient and cover transmittance. Type 50, mode 2, simulates a flat-plate photovoltaic thermal solar collector component with a single glazing sheet [22]. The model considers losses as a function of the temperature, wind speed and geometry, and constant cover transmittance. PV cell average temperature, T_{cell}, is calculated through an energy balance according to the modified Hottel–Whillier–Bliss equations [22]. The model calculates PVT electrical efficiency as a linear function of the T_{cell}, as follows in Equation (1):

$$\eta_{PV} = \eta_{PV,ref}\,[1 - \beta_{PV}\cdot(T_{cell} - T_{ref})] \quad (1)$$

$\eta_{PV,ref}$ is the reference efficiency of the PV module, βPV is a temperature coefficient, and T_{ref} is the reference temperature.

The thermal efficiency of the collector is expressed according to Equations (2) and (3):

$$\eta_{th} = FR\cdot(\tau\alpha) - FR\cdot U\cdot\frac{(T_{in} - T_{amb})}{G} \quad (2)$$

$$FR = \frac{m_f\cdot c_f}{U\cdot A_{PVT}}\cdot\left[1 - \exp\left(-\frac{U\cdot A_{PVT}\cdot F'}{m_f\cdot c_f}\right)\right] \quad (3)$$

A_{PVT} is the PVT collector area, T_{amb} is the ambient temperature, T_{in} is the inlet temperature, U is the overall collector heat loss, ($\tau\alpha$) is the transmission-absorption product, and G is the solar radiation. FR is the heat removal efficiency factor given as a function of the average mass flow rate (m_f), the heat capacity of the flowing medium (c_f), and the fin efficiency factor (F′) [36].

Finally, the PVT design parameters chosen for the case study analyzed in this paper are taken from Refs. [37,38] and are listed in Table 2.

2.2.2. Desiccant Air Conditioning Model

DAC is a cooling system that regulates both the temperature and moisture of the air supplied to a building. Thus, it can provide thermal comfort and hygienic conditions [39]. The most common configuration refers to the ventilation mode, enabling 100% indoor air renewal of the building, as seen in Figure 2.

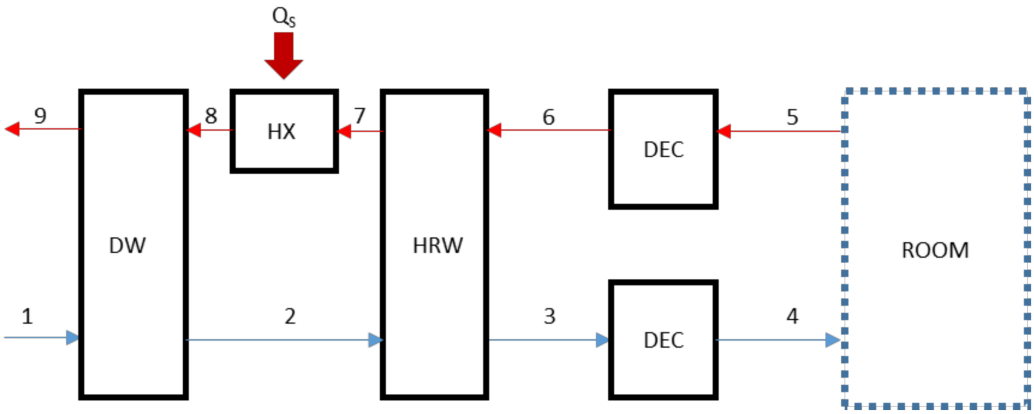

Figure 2. Desiccant air conditioning system (ventilation mode).

A complete desiccant air conditioning system is comprised of a desiccant wheel (DW), two direct evaporative coolers (DEC), and a heat recovery wheel (HRW). The system's operation starts with the DW dehumidifying and heating a supply of ambient air stream (1). At state (2), the process's airflow enters the HRW and is cooled down until state (3). It then passes through a DEC to be cooled down again and humidified, achieving the building's required thermal comfort conditions (4). In the counter flow, the building's exhaust air stream (5), dependent on the internal thermal load, enters the second DEC, where this airflow is first cooled down and then humidified to state (6). Thus, it can absorb sensible heat from the hot and dry process air stream through the HRW (7). At this point, the exhausted airflow needs to reach the regeneration temperature to provide for the DW regeneration. It is achieved by a heat exchanger (HX), releasing a flow at state (8).

Regarding the regeneration heat source, temperatures in the range of 50–80 °C present satisfactory effectiveness. Thus, it allows low-temperature solar thermal energy exploitation, such as with PVT collectors. Finally, the exhaust's air stream passes through the DW. It is cooled, humidified, and released to the environment at state (9) [25].

Another cycle also referred to in the relevant literature is the recirculation mode. According to this configuration (Figure 3), the supply airstream consists of the building's conditioned air.

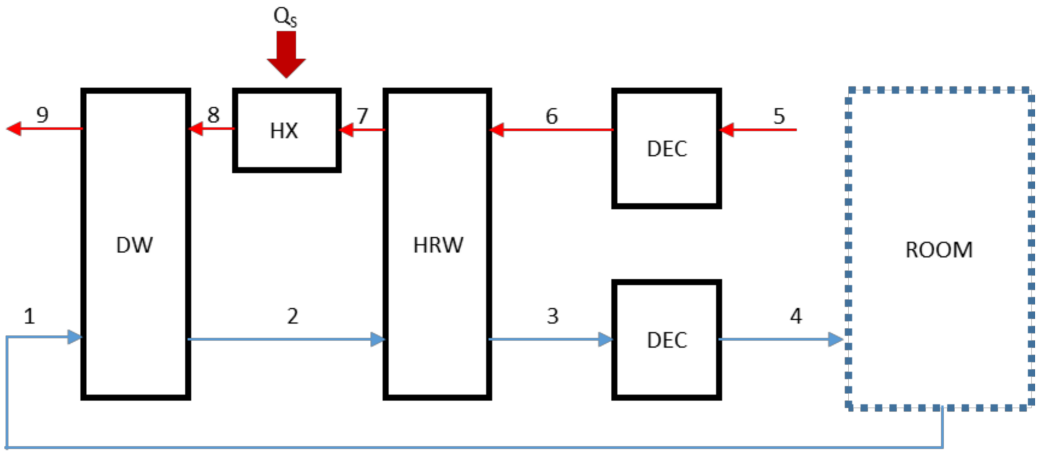

Figure 3. Desiccant air conditioning system (recirculation mode).

The DAC needs five model types for its proper operation in TRNSYS. Types 716 (desiccant wheel), 760 (heat recovery wheel), 506 (direct evaporative cooler), and 670 (heating coil) were used to perform the desiccant cooling system simulation. The DAC design parameters chosen are taken from Panaras et al. [25] and are listed in Table 2.

The main models included in the DAC system are detailed as follows:

Desiccant Wheel

The process's air stream flows through the desiccant material, which retains the moisture of the air. The desiccant capacity of this material can be restored through its regeneration. Type 716 models a rotary desiccant dehumidifier containing nominal silica gel whose performance is based on equations developed by Jurinak [40] for F1 and F2 potentials (ip = 1,2,8):

$$\mathrm{F1_{ip}} = \frac{-2865}{\left(T_{ip} + 273.15\right)^{1.49}} + 4.344 \times \left(\frac{w_{ip}}{1000}\right)^{0.8624} \quad (4)$$

$$\mathrm{F2_{ip}} = \frac{\left(T_{ip} + 273.15\right)^{1.49}}{6360} - 1.127 \times \left(\frac{w_{ip}}{1000}\right)^{0.07969} \quad (5)$$

$$\eta \mathrm{F_1} = \frac{\mathrm{F1_2} - \mathrm{F1_2}}{\mathrm{F1_8} - \mathrm{F1_1}} \quad (6)$$

$$\eta \mathrm{F_2} = \frac{\mathrm{F2_2} - \mathrm{F2_1}}{\mathrm{F2_8} - \mathrm{F2_1}} \quad (7)$$

It is important to note that the efficiency factor η_{F1} represents the process's approximation to an adiabatic one, whereas the η_{F2} expresses the dehumidification degree.

Heat Recovery Wheel

Type 760 uses the constant effectiveness –minimum capacitance approach (ε_{HRW}) to model this air-to-air heat exchanger. It should be noted that it transfers only sensible energy during its operation [41]:

$$\varepsilon_{\mathrm{HRW}} = \frac{\mathrm{T_2} - \mathrm{T_3}}{\mathrm{T_2} - \mathrm{T_6}} = \frac{\mathrm{T_6} - \mathrm{T_7}}{\mathrm{T_6} - \mathrm{T_2}} \quad (8)$$

Direct Evaporative Cooler

This model (Type 506) cools an inlet air stream by passing it through a wetted surface, evaporating the water from the surface, and cooling the air stream in the process. The ideal exiting air state for a DEC is if it exits with a dry-bulb temperature equal to its inlet

wet-bulb temperature. It takes the humidity efficiency of the device to calculate the air outlet conditions [22]:

$$\varepsilon_{DEC} = \frac{T_{ip} - T_{ip+1}}{T_{ip} - T_{wb,ip}} \quad (9)$$

ip = 3 for the supply stream humidifier and ip = 5 for the exhaust stream humidifier, and wb is the wet-bulb temperature. Furthermore, Type 506 considers the DEC water consumption as negligible.

Heat Exchanger

Type 670 simulates an air-heating coil (regenerator). The exhausted airflow is heated to provide for the regeneration of the desiccant wheel. It takes the full effectiveness of the device to reach the regeneration temperature. It can be stated that desiccant systems present good thermal effectiveness for a range of regeneration temperatures relevant to the use of simple flat-plate solar collectors [25].

Finally, the coefficient of performance (COP) of the desiccant cooling system is evaluated for the ventilation mode [42]. The purpose of the machine is to cool the building, and to this end, it consumes the regeneration energy:

$$COP = \frac{m_{a,sup} \cdot (h_5 - h_4)}{m_{a,ret} \cdot (h_8 - h_7)} \quad (10)$$

If recirculation mode is considered, the enthalpy of state 5 is replaced by state 1.

2.2.3. Thermal Comfort

TRNSYS includes a built-in subroutine to perform the thermal comfort analysis of building users. This model is developed according to the International Standard Organization's (ISO) 7730 standard [43], described in detail by Fanger [44]. It establishes a statistical correlation between the Predicted Mean Vote (PMV) thermal comfort index and the thermal load acting on the human body:

$$PMV = L\,(0.0303e^{-0.036\,M} + 0.028) \quad (11)$$

The PMV index is calculated according to the energy loss to the environment (L) and the user's metabolic rate (M). It predicts a group of occupants' ambient thermal comfort sensation by the mean value of votes. The index is translated as +3 for a too-hot sensation and −3 for a too-cold feeling. The 0 value represents a neutral comfort condition. To measure the satisfaction level of the occupants in an ambient setting, Fanger developed the Predicted Percentage of Dissatisfied (PPD) index, defined as follows:

$$PPD = 100 - 95e^{-(0.03353\,PMV^4 + 0.2179\,PMV^2)} \quad (12)$$

The TRNBULD comfort subroutine calculates PMV and PPD as a function of the ambient climatic conditions and the person-specific parameters. Regarding the person-specific parameters, metabolism rate, clothing insulation, and air velocity were taken from ASHRAE Standard 55 [45], as shown in Table 3.

Table 3. Thermal comfort parameters.

Parameter	Description	Factor
Clothing factor [clo]	Light outdoor sportswear	0.9
Metabolic rate [met]	Seated, light work	1.2
Air velocity [m/s]	Still air	0.2

2.2.4. Energy Model

The Primary Energy Saving (PES) evaluates the energy performance of the proposed system (PS) through a comparison with a suitable reference system (RS). The PS solely considers the demand unattended to by renewable energy sources. On the other hand, the RS supposes all demands are produced by conventional technologies based on fossil fuels. It is worth noting that electricity demand already aggregates freshwater demand. The reference technologies were an electric vapor compression air conditioning (VC) system with an average coefficient of performance, COP_{VC}, of 2.6, and a natural gas boiler (GB) with average thermal efficiency, η_{th}, of 0.92 [46]. The national grid efficiency was taken from the Spanish resolution published by IDAE [47], η_{el} = 0.42.

The PES and its ratio (PES_R) are calculated as shown in Equations (13) and (14):

$$PES = PE_{RS} - PE_{PS} \quad (13)$$

$$PES_R = \frac{PES}{PE_{RS}} \quad (14)$$

$$PE_{RS} = \left(\frac{P_{Build,\,dem} + P_{Syst,\,dem}}{\eta_{el}} + \frac{Q_{DHW,\,dem} + Q_{Heat,\,dem}}{\eta_{th}} + \frac{Q_{Cool,\,dem}}{COP_{VC} \cdot \eta_{el}} \right)_{RS} \quad (15)$$

$$PE_{PS} = \left(\frac{P_{Grid,aux}}{\eta_{el}} + \frac{Q_{DHW,\,aux} + Q_{Heat,\,aux}}{\eta_{th}} + \frac{Q_{Cool,\,aux}}{COP_{VC} \cdot \eta_{el}} \right)_{PS} \quad (16)$$

$P_{Grid,aux}$ is the electric energy withdrawn from the national grid to meet PS electricity demand, and $Q_{DHW,aux}$, $Q_{Heat,aux}$, and $Q_{Cool,aux}$ are the thermal energy demands required to be supplied by an auxiliary GB for DHW and space heating, and by a VC for space cooling, respectively.

2.2.5. Environmental Model

Similarly, the environmental analysis was evaluated by the saving in CO_2 emissions and its ratio (CO_{2R}) as showed in Equations (17) and (18):

$$CO_2 = CO_{2RS} - CO_{2PS} \quad (17)$$

$$CO2_R = \frac{CO_2}{CO_{2RS}} \quad (18)$$

$$CO_{2RS} = \left[\left(P_{Build,dem} + P_{Syst,dem} \right) \cdot f_{CO_2,EE} + \left(Q_{DHW,dem} + Q_{Heat,dem} \right) \cdot f_{CO_2,NG} + \left(\frac{Q_{Cool,dem}}{COP_{VC}} \right) \cdot f_{CO_2,EE} \right]_{RS} \quad (19)$$

$$CO_{2PS} = \left[\left(P_{Grid,aux} \right) \cdot f_{CO_2,EE} + \left(Q_{DHW,aux} + Q_{Heat,aux} \right) \cdot f_{CO_2,NG} + \left(\frac{Q_{Cool,aux}}{COP_{VC}} \right) \cdot f_{CO_2,EE} \right]_{PS} \quad (20)$$

The CO_2 emission factor of natural gas consumption, $f_{CO_2,NG}$, in Spain is 0.25 $kgCO_2/kWh$ [47]. In the case of the Spanish national grid, $f_{CO_2,EE}$, *REE* [48] provides the emission factor associated with electricity generation, 0.19 $kgCO_2/kWh$.

3. Results

Case study demands are deeply reported by Gesteira et al. [49]. It refers to a single-family townhouse located in the city of Almería, in the Mediterranean European side of Spain. Due to its high summer humidity and, therefore, high cooling latent load, it is suitable for the application of desiccant cooling systems. In these systems, the sensible and latent loads are controlled independently. The latent heat is reduced without cooling the air below its dew point, which is a great advantage [28]. Meteonorm weather data for Almería (36°50′17″ N, 2°27′35″ W) were used for climatic data acquisition.

The dynamic simulation returns temperature, energy, and flowrate profiles, with instantaneous or integrated values. The simulation was performed based on a 1-year time span (from 0 h to 8760 h) with a 5-min time step. This time step allows the controllers to work correctly. First, a design optimization study evaluates the optimal system configuration. For that reason, some design parameters are related to each other. In particular, the PVT field area automatically determines the solar pump flowrate and the TES volume (Table 2). Finally, the dynamic behavior of the optimal system is presented in terms of temperature and energy profiles for representative days of winter and summer. The yearly results show the main performance metrics, and a comparative study with an alternative coastal location is also included to extend the viability of the proposed system.

3.1. Design Optimization

A parametric analysis was developed to provide the optimal system design. In particular, the optimal configuration is obtained when all demands achieve their maximum coverage. The following demand coverages were chosen for the study: electric (C_{El}), heating (C_{Heat}), cooling (C_{Cool}), and DHW (C_{DHW}). The freshwater coverage uses the grid as a backup. Thus, it achieves 100% in all cases. The most critical design parameter of a solar system is the field area, which is related to energy production. For that reason, the sensitivity of the coverages was analyzed as a function of the PVT's size (A_{PVT}). The area varied from 5 m^2 to 30 m^2. Figure 4 shows the parametric study.

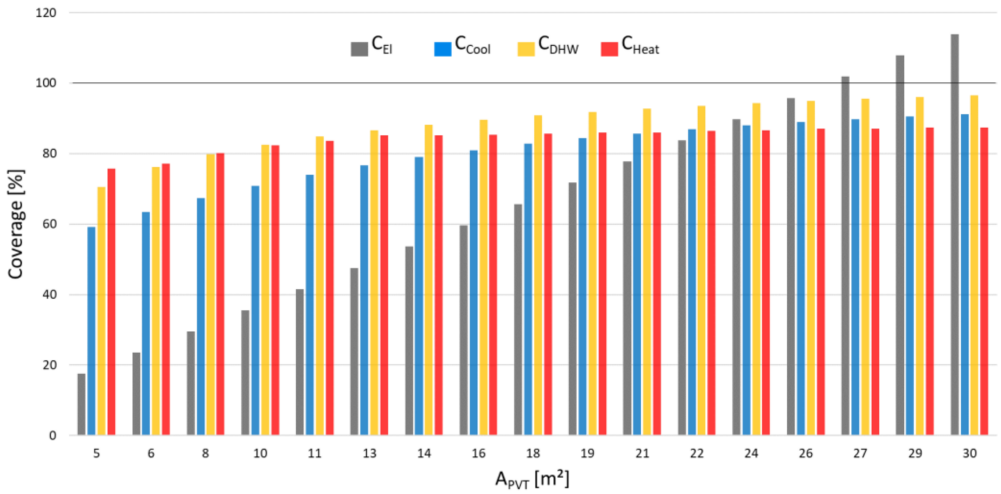

Figure 4. Parametric analysis: performance parameters, PVT collector area.

The increase in the PVT's area directly affects the C_{El}, and realizes 100% at 27.2 m^2 of A_{PVT}. An annual near-zero energy balance for the electricity is desired during the simulation. Consequently, there is no energy convenience in increasing the PVT collectors' area over 27.2 m^2 once 100% electric coverage is already achieved with a slight electricity surplus. It is worth noting that the increase in electric energy produced by the PVT collectors and not utilized by the building determines the non-refundable electricity injected into the grid.

Another relevant parameter for design optimization is the $T_{TES,top}$ setpoint. The AH cools the SCF down whenever the PVT's outlet temperature increases the $T_{TES,top}$ over the setpoint. It controls the SCF temperature and, consequently, the PVT efficiency. Moreover, it determines the available thermal energy for heating, cooling, and DHW. However, the mainly impacted coverage in this study was the cooling coverage. Thus, the parametric study analyzed the cooling coverage versus the PVT efficiency as a function of the $T_{TES,top}$ setpoint. The temperature varied from 50 °C to 80 °C, which is a suitable temperature range for the system's thermal needs. Figure 5 shows the parametric study.

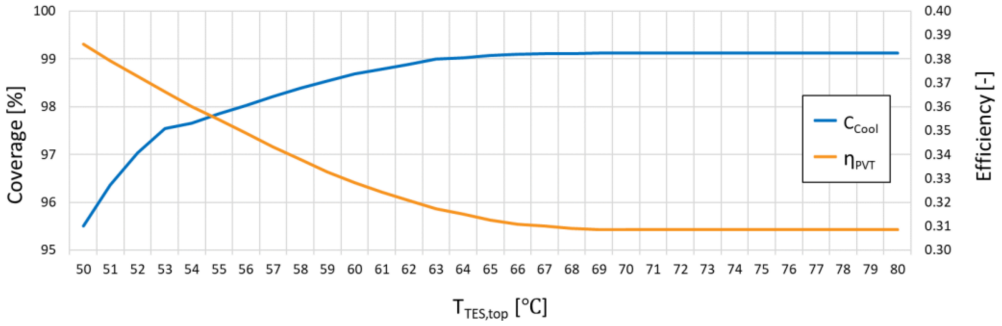

Figure 5. Parametric analysis: cooling coverage versus PVT efficiency, TES top temperature.

The increase in TES's top temperature setpoint directly affects the C_{Cool}, as the greater available thermal energy increases the efficiency of the desiccant wheel. However, it reduces the PVT efficiency due to higher thermal losses (higher mean temperature of the SCF entering the collectors). Thus, the optimal $T_{TES,top}$ setpoint that ensures a sufficient cooling coverage and PVT efficiency is achieved at 55 °C.

Finally, the study compared the ventilation and recirculation modes on the efficiency and coverage metrics (Table 4). The COP_{DAC} showed an enhancement in the ventilation mode, 0.47, against 0.44 for the recirculation case. Thus, the ventilation mode was selected as the optimal DAC configuration.

Table 4. Ventilation vs. recirculation modes.

			Ventilation	**Recirculation**
Parameter	**Symbol**	**Unit**	**Value**	
PVT total efficiency	η_{PVT}	–	0.35	0.35
DAC thermal COP	COP_{DAC}	–	0.47	0.44
Electricity coverage	C_{El}	%	104.1	101.32
DHW coverage	C_{DHW}	%	96.05	95.48
Heating coverage	C_{Heat}	%	87.01	87.01
Cooling coverage	C_{Cool}	%	97.98	97.85
Freshwater coverage	C_{FW}	%	100	100

3.2. Daily Analysis: A Typical Summer Day

It presents the daily results provided by the simulation for the cooling season. As a representative day, 6 August (from 5208 h to 5232 h) was selected. Figure 6 displays the profile of the main parameters for the representative summer day. The outlet temperature of the PVT collectors ($T_{PVT,out}$) follows the solar thermal gain. $T_{PVT,out}$ starts to increase at 6:30 a.m., reaches its maximum at 2:30 p.m., and then decreases until 8:00 p.m. The TES's top temperature ($T_{TES,top}$) rises from 51 °C to its setpoint (55 °C) during the daylight. Consequently, the air heater signal (y_{AH}) is activated, and heat is dissipated to the environment between 2:30 p.m. and 5:00 p.m. It is worth noting that, during AH activation, the reduction in the SCF's temperature increases the PVT's efficiency; thus, the $T_{PVT,out}$ presents several peaks and valleys.

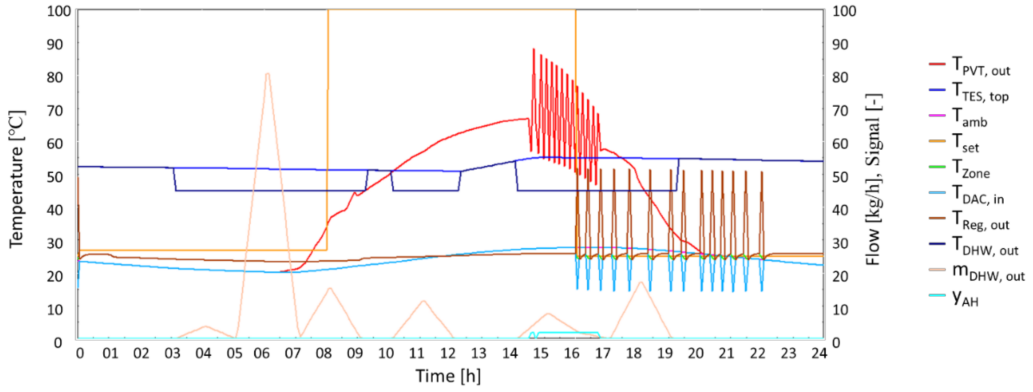

Figure 6. Summer day profile.

The ambient temperature (T_{amb}) varies from 20 °C at 6:00 a.m. to 28 °C at 4:00 p.m. During the morning, due to a mild ambient temperature, the thermostat does not activate cooling. According to the Spanish technical building code (BD-ES) [46], the thermostat setpoint temperature (T_{set}) during the mornings is 27 °C. However, the building's thermal gains increase throughout the day, so cooling is required in the afternoon after 4:00 p.m. This demand also occurs because of the reduction in the T_{set} to 25 °C. The DAC system provides for space cooling, blowing cool air inside the building at 14 °C ($T_{DAC,in}$) and thus reducing the building's zone temperature (T_{Zone}) to 25 °C during the system's operation. T_{Zone} remains around the T_{set} with a dead band of ±1 °C. Moreover, for the desiccant wheel's proper regeneration, the TES thermal energy feeds the regenerator and raises its outlet airflow temperature ($T_{Reg,out}$) up to 51 °C.

Regarding the DHW, the outlet temperature ($T_{DHW,out}$) and the outlet mass flow ($m_{DHW,out}$) are presented. $T_{DHW,out}$ meets the required temperature of 45 °C from 3:00 a.m. to 9:00 a.m., from 10:00 a.m. to 12:30 a.m., and from 2:00 p.m. to 7:30 p.m.

3.3. Daily Analysis: A Typical Winter Day

The selected winter day provided by the simulation in the heating season was 24 January (from 552 h to 576 h). Figure 7 shows the main parameters for the system on the selected day. Here, the solar loop presents a shorter sunlight period. $T_{PVT,out}$ starts to increase at 8:30 a.m., reaches its maximum value at 2:30 p.m. and then decreases until 6:00 p.m., lasting about four hours less than in the summertime. The $T_{TES,top}$ increases from 50 °C to 53 °C during daylight. The AH is not activated during the winter due to lower solar radiation.

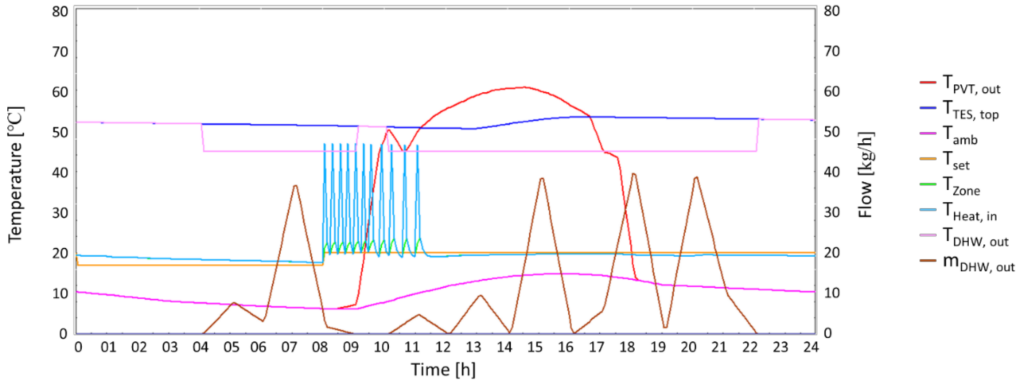

Figure 7. Winter day profile.

T_{amb} achieves its minimum at 9:00 am (6 °C) and maximum at 3:30 pm (15 °C). During the morning, due to a temperature decrease throughout the night and the increase of T_{set} from 17 °C to 20 °C at 8:00 a.m. [46], the thermostat activates heating from 8:00 a.m.

to 11:00 a.m. In the afternoon, the building gains (solar irradiation, occupancy, lighting, and equipment) increase the indoor temperature. Thus, no heating is required. T_{Zone} remains around the T_{set} throughout the day with a dead band of ±1 °C. The heating system provides for space heating, blowing airflow into the building at 47 °C ($T_{Heat,in}$).

Finally, $T_{DHW,out}$ meets the required temperature of 45 °C from 4:00 a.m. to 9:00 a.m. and from 10:00 a.m. to 10:00 p.m., according to the $m_{DHW,out}$ demand.

3.4. Yearly Results

The annual simulation results (from 0 h to 8760 h) are summarized in Table 5. In this table, the integrated amounts of electricity, heat, and water volume are shown for one year. In particular, the building demands were estimated in Ref. [49]. The total electricity demand ($P_{Tot,dem}$) is the sum of the building ($P_{Build,dem}$) and the system's ($P_{Syst,dem}$) electricity demands. The total water demand ($m_{Tot,dem}$) is the sum of the DHW ($m_{DHW,dem}$) and freshwater ($m_{FW,dem}$) demands. The total thermal demand ($Q_{Tot,dem}$) is comprised of the DHW thermal demand ($Q_{DHW,dem}$) and the cooling ($Q_{Cool,dem}$) and heating ($Q_{Heat,dem}$) demands. Note that $Q_{Cool,dem}$ is higher than $Q_{Heat,dem}$ due to local weather conditions.

Table 5. Yearly results.

Parameter	Symbol	Value	Unit
Building electricity demand	$P_{Build,dem}$	3866	kWh/yr [49]
System electricity demand	$P_{Syst,dem}$	1066	kWh/yr
Total electricity demand	$P_{Tot,dem}$	4932	kWh/yr
DHW demand	$m_{DHW,dem}$	41	m^3/yr [49]
Freshwater demand	$m_{FW,dem}$	110	m^3/yr [49]
Total water demand	$m_{Tot,dem}$	151	m^3/yr
DHW thermal demand	$Q_{DHW,dem}$	1260	kWh/yr
Building cooling demand	$Q_{Cool,dem}$	1450	kWh/yr [49]
Building heating demand	$Q_{Heat,dem}$	941	kWh/yr [49]
Total thermal demand	$Q_{Tot,dem}$	3651	kWh/yr
PVT power production	P_{PVT}	5701	kWh/yr
Power losses	P_{Loss}	570	kWh/yr
Total power production	P_{Tot}	5131	kWh/yr
PVT heat production	Q_{PVT}	8990	kWh/yr
Air heater dissipation	Q_{AH}	1857	kWh/yr
Heat losses	Q_{Loss}	1993	kWh/yr
Total useful heat production	Q_{Tot}	5140	kWh/yr
RO freshwater production	m_{RO}	151	m^3/yr

The total power production ($P_{Tot,prod}$) is the PVT power production (P_{PVT}) minus the power loss (P_{Loss}) wasted by the inverter due to its inefficiency during DC to AC conversion (10%). If $P_{Tot,prod}$ is insufficient for attending $P_{Tot,dem}$, electricity can be withdrawn from the national grid. On the other hand, if $P_{Tot,dem}$ exceeds $P_{Tot,prod}$, electricity can be injected into the national grid. An annual near-zero electricity balance is achieved during the simulation.

The total useful heat (Q_{Tot}) is the PVT heat production (Q_{PVT}) minus the heat dissipated by the AH (Q_{AH}) and the heat loss to the environment by the system devices (Q_{Loss}). The energy dissipated by the air heater is around 20.7%, and the thermal losses correspond to 22% of Q_{PVT}. The air heater activates mainly during the autumn and spring due to the lower thermal energy consumption, and during the summer because of the higher solar radiation.

As shown in Table 6, Q_{Tot} is used for attending $Q_{DHW,dem}$, $Q_{Cool,dem}$, and $Q_{Heat,dem}$.

Table 6. Thermal production breakdown.

Parameter	Symbol	Value	Unit
DHW consumption	Q_{DHW}	1210	kWh/yr
Heating coil exchanger	Q_{HX}	798	kWh/yr
DAC regenerator	Q_{Reg}	3000	kWh/yr

Finally, Table 7 presents the energy and environmental results for the proposed polygeneration system.

Table 7. Energy and environmental results.

Parameter	Symbol	Unit	Value
Primary energy saving ratio	PES_R	%	98.62
CO_2 saving ratio	CO_{2R}	%	97.17

3.5. Thermal Comfort

The thermal comfort analysis of the case study is reported in Ref. [49]. It presented two different situations: no indoor temperature control and temperature control as defined by the BD-ES [46]. Here, the thermal comfort of the same case study is provided by the polygeneration system. In particular, Figure 8 shows the thermal comfort analysis described by the PMV and PPD indexes.

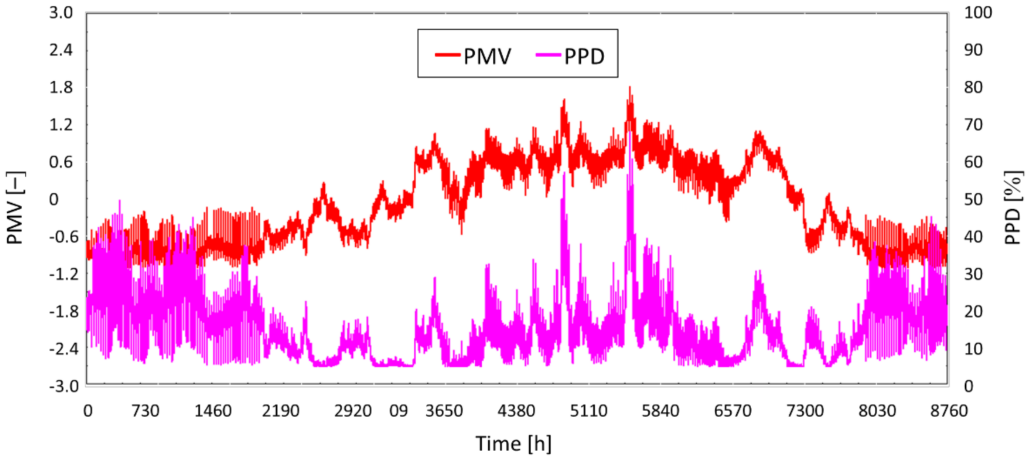

Figure 8. Thermal comfort analysis.

PMV ranges between −1.3 and 1.6 throughout the year, which can be explained as a slightly cool sensation during the winter and a warm feeling during the summer. Consequently, the PPD index presents a maximum occupant dissatisfaction rate of 42% during the winter and 63% in the summer. The thermal comfort analysis showed a remarkable improvement all year long compared to the case study without controls.

3.6. Comparison between Almería and an Alternative Coastal City

The polygeneration system was also applied to an alternative coastal city to evaluate its feasibility. Therefore, Valencia was selected, as it is located along the Spanish Mediterranean coast and presents different climate conditions. Valencia is characterized by lower horizontal global solar radiation per year and over twice the demand for heating (1828 kWh/yr) and slightly more for cooling (1567 kWh/yr) than Almería. By using the previously described methodology, the optimal system configuration was selected for the PVT collectors' area equal to 32 m^2 and a TES top temperature of 57 °C. The comparison between both cities is summarized in Table 8.

Table 8. Almería vs. Valencia efficiency parameters.

			Almería	Valencia
Parameter	**Symbol**	**Unit**	**Value**	
PVT total efficiency	η_{PVT}	–	0.35	0.35
DAC thermal COP	COP_{DAC}	–	0.47	0.47
Electricity coverage	C_{El}	%	104.1	105.7
DHW coverage	C_{DHW}	%	96.05	90.15
Heating coverage	C_{Heat}	%	87.01	87.31
Cooling coverage	C_{Cool}	%	97.98	97.9
Freshwater coverage	C_{FW}	%	100	100
Primary energy saving ratio	PES_R	%	98.62	97.57
CO_2 saving ratio	CO_{2R}	%	97.17	95.04

Valencia needs a higher PVT collectors' area due to the lower horizontal global solar radiation per year. Furthermore, as it demands more heating and cooling, it thus justifies the increase in the TES's top temperature. The PVT efficiency (η_{PVT}) and the yearly mean COP_{DAC} for both cities are equal, 0.35 and 0.47, respectively. Finally, the polygeneration system applied to Almería presents an advantage in energy and environmental results.

4. Discussion

This work presented a novel simulation of a polygeneration system for residential electricity, heating, cooling, domestic hot water, and freshwater production. The proposed system integrates a solar-assisted desiccant air conditioning system for cooling purposes. The system was applied to a single-family townhouse located on the Mediterranean European side of Spain. The system can be applied to a similar area with moderate relative humidity and ambient temperature, which allows for the operation of desiccant air conditioning. The system's layout was dynamically simulated in the TRNSYS environment by developing comprehensive models suitable for evaluating the transient energy performance (temperatures, heat, power, and efficiency) of all the system's components on an hourly and yearly basis. Design optimization of the system was also performed under different conditions to determine the optimal size for attending to dwelling demands. The main findings of the simulations are summarized in the following:

1. The optimal system configuration for Almería was obtained at a photovoltaic/thermal collector's area of 27.2 m^2 and a top temperature for thermal energy storage of 55 °C;
2. The yearly results showed that the energy dissipated by the air heater is around 20.7% of the produced heat. The device activates mainly during the autumn, spring, and summer due to the lower thermal energy consumption or higher solar radiation;
3. The thermal comfort analysis showed a remarkable improvement compared to the results of the case study performed without temperature controls;
4. Comparing the results for the cities Almería and Valencia, it can be concluded that Valencia presents similar results to Almería. Thus, the proposed polygeneration system works correctly and is reliable.

Finally, the developed polygeneration system showed to be replicable for other cities and introduced solar-assisted desiccant cooling technology for the residential sector. It can be a promising solution for attending to energy demands using renewable energy sources. Further studies will develop an economic analysis and a multiobjective optimization for the proposed system.

Author Contributions: Conceptualization, J.U.; methodology, L.G.G.; formal analysis, L.G.G.; investigation, L.G.G.; resources, J.U.; data curation, L.G.G.; writing—original draft preparation, L.G.G.; writing—review and editing, L.G.G. and J.U.; supervision, J.U. All authors have read and agreed to the published version of the manuscript.

Funding: This research received no external funding.

Institutional Review Board Statement: Not applicable.

Informed Consent Statement: Not applicable.

Data Availability Statement: Not applicable.

Conflicts of Interest: The authors declare no conflict of interest.

References

1. International Energy Agency (IEA), Energy and Climate Change–World Energy Outlook Special Report, Paris. 2015. Available online: https://www.iea.org/reports/energy-and-climate-change (accessed on 9 March 2020).
2. European Commission, Communication from the Commission to the European Parliament, the Council, the European Economic and Social Committee and the Committee of the Regions—An EU Strategy on Heating and Cooling, Brussels. 2016. Available online: https://ec.europa.eu/energy/sites/ener/files/documents/1_EN_ACT_part1_v14.pdf (accessed on 6 April 2020).
3. European Commission. Commission Recommendation (Eu) 2016/1318-on Guidelines for the Promotion of Nearly Zero-Energy Buildings and Best Practices to Ensure that, by 2020, All New Buildings Are Nearly Zero-Energy Buildings. *Off. J. Eur. Union* **2016**, *L 208*, 46–57.
4. Costa, A.; Keane, M.M.; Torrens, J.I.; Corry, E. Building operation and energy performance: Monitoring, analysis and optimization toolkit. *Appl. Energy* **2013**, *101*, 310–316. [CrossRef]
5. European Commission. *SET-Plan ACTION n°5-ISSUES PAPER-Develop New Materials and Technologies for Energy Efficiency Solutions for Buildings*; SET Plan Secretariat: Brussels, Belgium, 2016.
6. Calise, F.; de Notaristefani di Vastogirardi, G.; Dentice d'Accadia, M.; Vicidomini, M. Simulation of polygeneration systems. *Energy* **2018**, *163*, 290–337. [CrossRef]
7. Buonomano, A.; Calise, F.; Palombo, A.; Vicidomini, M. Energy and economic analysis of geothermal-solar trigeneration systems: A case study for a hotel building in Ischia. *Appl. Energy* **2015**, *138*, 224–241. [CrossRef]
8. Calise, F.; d'Accadia, M.D.; Libertini, L.; Quiriti, E.; Vicidomini, M. A novel tool for thermoeconomic analysis and optimization of trigeneration systems: A case study for a hospital building in Italy. *Energy* **2017**, *126*, 64–87. [CrossRef]
9. Calise, F.; d'Accadia, M.D.; Figaj, R.D.; Vanoli, L. A novel solar-assisted heat pump driven by photovoltaic/thermal collectors: Dynamic simulation and thermoeconomic optimization. *Energy* **2016**, *95*, 346–366. [CrossRef]
10. Carotenuto, A.; Figaj, R.D.; Vanoli, L. A novel solar-geothermal district heating, cooling and domestic hot water system: Dynamic simulation and energy-economic analysis. *Energy* **2017**, *141*, 2652–2669. [CrossRef]
11. Angrisani, G.; Entchev, E.; Roselli, C.; Sasso, M.; Tariello, F.; Yaïci, W. Dynamic simulation of a solar heating and cooling system for an office building located in Southern Italy. *Appl. Therm. Eng.* **2016**, *103*, 377–390. [CrossRef]
12. Calise, F. Thermoeconomic analysis and optimization of high efficiency solar heating and cooling systems for different Italian school buildings and climates. *Energy Build.* **2010**, *42*, 992–1003. [CrossRef]
13. Serra, L.M.; Lozano, M.-A.; Ramos, J.; Ensinas, A.V.; Nebra, S.A. Polygeneration and efficient use of natural resources. *Energy* **2009**, *34*, 575–586. [CrossRef]
14. Jana, K.; Ray, A.; Majoumerd, M.M.; Assadi, M.; De, S. Polygeneration as a future sustainable energy solution—A comprehensive review. *Appl. Energy* **2017**, *202*, 88–111. [CrossRef]
15. Acevedo, L.; Uche, J.; del Almo, A.; Círez, F.; Usón, S.; Martínez, A.; Guedea, I. Dynamic Simulation of a Trigeneration Scheme for Domestic Purposes Based on Hybrid Techniques. *Energies* **2016**, *9*, 1013. [CrossRef]
16. Uche, J.; Acevedo, L.; Círez, F.; Usón, S.; Martínez-Gracia, A.; Bayod-Rújula, Á.A. Analysis of a domestic trigeneration scheme with hybrid renewable energy sources and desalting techniques. *J. Clean. Prod.* **2019**, *212*, 1409–1422. [CrossRef]
17. Usón, S.; Uche, J.; Martínez, A.; del Amo, A.; Acevedo, L.; Bayod, Á. Exergy assessment and exergy cost analysis of a renewable-based and hybrid trigeneration scheme for domestic water and energy supply. *Energy* **2019**, *168*, 662–683. [CrossRef]
18. Elmer, T.; Worall, M.; Wu, S.; Riffat, S. An experimental study of a novel integrated desiccant air conditioning system for building applications. *Energy Build.* **2016**, *111*, 434–445. [CrossRef]
19. Angrisani, G.; Minichiello, F.; Roselli, C.; Sasso, M. Desiccant HVAC system driven by a micro-CHP: Experimental analysis. *Energy Build.* **2010**, *42*, 2028–2035. [CrossRef]
20. Jani, D.B.; Mishra, M.; Sahoo, P.K. Performance analysis of a solid desiccant assisted hybrid space cooling system using TRNSYS. *J. Build. Eng.* **2018**, *19*, 26–35. [CrossRef]
21. Elgendy, E.; Mostafa, A.; Fatouh, M. Performance enhancement of a desiccant evaporative cooling system using direct/indirect evaporative cooler. *Int. J. Refrig.* **2015**, *51*, 77–87. [CrossRef]
22. *TRNSYS: A Transient System Simulation Program*; Solar Energy Laboratory, University of Wisconsin: Madison, WI, USA, 2006.
23. Angrisani, G.; Minichiello, F.; Sasso, M. Improvements of an unconventional desiccant air conditioning system based on experimental investigations. *Energy Convers. Manag.* **2016**, *112*, 423–434. [CrossRef]
24. Sopian, K.; Dezfouli, M.M.S.; Mat, S.; Ruslan, M.H. Solar Assisted Desiccant Air Conditioning System for Hot and Humid Areas. *Int. J. Environ. Sustain.* **2014**, *3*, 23–32. [CrossRef]
25. Panaras, G.; Mathioulakis, E.; Belessiotis, V. Solid desiccant air-conditioning systems—Design parameters. *Energy* **2011**, *36*, 2399–2406. [CrossRef]

26. Fabrizio, E.; Seguro, F.; Filippi, M. Integrated HVAC and DHW production systems for Zero Energy Buildings. *Renew. Sustain. Energy Rev.* **2014**, *40*, 515–541. [CrossRef]
27. Farooq, A.S.; Badar, A.W.; Sajid, M.B.; Fatima, M.; Zahra, A.; Siddiqui, M.S. Dynamic simulation and parametric analysis of solar assisted desiccant cooling system with three configuration schemes. *Sol. Energy* **2020**, *197*, 22–37. [CrossRef]
28. Heidari, A.; Roshandel, R.; Vakiloroaya, V. An innovative solar assisted desiccant-based evaporative cooling system for co-production of water and cooling in hot and humid climates. *Energy Convers. Manag.* **2019**, *185*, 396–409. [CrossRef]
29. Villarruel-Jaramillo, A.; Pérez-García, M.; Cardemil, J.M.; Escobar, R.A. Review of Polygeneration Schemes with Solar Cooling Technologies and Potential Industrial Applications. *Energies* **2021**, *14*, 6450. [CrossRef]
30. Pina, E.A.; Lozano, M.A.; Serra, L.M. A multiperiod multiobjective framework for the synthesis of trigeneration systems in tertiary sector buildings. *Int. J. Energy Res.* **2020**, *44*, 1140–1166. [CrossRef]
31. Melgar, S.G.; Cordero, A.S.; Rodríguez, M.V.; Márquez, J.M.A. Matching Energy Consumption and Photovoltaic Production in a Retrofitted Dwelling in Subtropical Climate without a Backup System. *Energies* **2020**, *13*, 6026. [CrossRef]
32. Pinto, E.S.; Serra, L.M.; Lázaro, A. Optimization of the design of polygeneration systems for the residential sector under different self-consumption regulations. *Int. J. Energy Res.* **2020**, *44*, 11248–11273. [CrossRef]
33. Ghalavand, Y.; Hatamipour, M.S.; Rahimi, A. A review on energy consumption of desalination processes. *Desalin. Water Treat.* **2015**, *54*, 1526–1541. [CrossRef]
34. Chow, T.T. A review on photovoltaic/thermal hybrid solar technology. *Appl. Energy* **2010**, *87*, 365–379. [CrossRef]
35. Zondag, H. Flat-plate PV-Thermal collectors and systems: A review. *Renew. Sustain. Energy Rev.* **2008**, *12*, 891–959. [CrossRef]
36. Fudholi, A.; Sopian, K.; Yazdi, M.H.; Ruslan, M.H.; Ibrahim, A.; Kazem, H.A. Performance analysis of photovoltaic thermal (PVT) water collectors. *Energy Convers. Manag.* **2014**, *78*, 641–651. [CrossRef]
37. Calise, F.; Figaj, R.D.; Vanoli, L. A novel polygeneration system integrating photovoltaic/thermal collectors, solar assisted heat pump, adsorption chiller and electrical energy storage: Dynamic and energy-economic analysis. *Energy Convers. Manag.* **2017**, *149*, 798–814. [CrossRef]
38. Zenhäusern, D.; Bamberger, E.; Baggenstos, A.; Häberle, A. PVT Wrap-Up: Energy Systems with Photovoltaic Thermal Solar Collectors. In Proceedings of the IEA SHC International Conference on Solar Heating and Cooling for Buildings and Industry, Abu Dhabi, United Arab Emirates, 29 October–2 November 2017; pp. 1–12. [CrossRef]
39. Rafique, M.M.; Gandhidasan, P.; Rehman, S.; Al-Hadhrami, L.M. A review on desiccant based evaporative cooling systems. *Renew. Sustain. Energy Rev.* **2015**, *45*, 145–159. [CrossRef]
40. Jurinak, J.J. Open Cycle Solid Desiccant Cooling–Component Models and System Simulations. Ph.D. Thesis, University of Wisconsin-Madison, Madison, WI, USA, 1982.
41. Panaras, G.; Mathioulakis, E.; Belessiotis, V.; Kyriakis, N. Theoretical and experimental investigation of the performance of a desiccant air-conditioning system. *Renew. Energy* **2010**, *35*, 1368–1375. [CrossRef]
42. Bourdoukan, P.; Wurtz, E.; Joubert, P. Experimental investigation of a solar desiccant cooling installation. *Sol. Energy* **2009**, *83*, 2059–2073. [CrossRef]
43. International Organization for Standardization (ISO). *ISO 7730:1994, Moderate Thermal Environments—Determination of the PMV and PPD Indices and Specification of the Conditions for Thermal Comfort*; ISO Standard: Geneva, Switzerland, 1994; p. 26.
44. Fanger, P.O. *Thermal Comfort. Analysis and Applications in Environmental Engineering*; Danish Technical Press: Copenhagen, Denmark, 1970.
45. *ANSI/ASHRAE Standard 55*; Thermal Environmental Conditions for Human Occupancy. The Society: New York, NY, USA, 2013.
46. Spanish Ministry of Development. Updating of the Energy Saving Document DB-HE of the Technical Building Code. 2019. Available online: https://www.codigotecnico.org/pdf/Documentos/HE/DBHE.pdf (accessed on 1 October 2021).
47. Instituto para la Diversificación y Ahorro de la Energía (IDAE). CO2 Emission Factors and Primary Energy Coefficients for Different Final Energy Sources Consumed in the Building Sector in Spain. 2014. Available online: https://energia.gob.es/desarrollo/EficienciaEnergetica/RITE/Reconocidos/Reconocidos/Otros%20documentos/Factores_emision_CO2.pdf (accessed on 15 February 2022).
48. Red Eléctrica Española (REE). CO2 Emissions of Electricity Generation in Spain. 2021. Available online: https://api.esios.ree.es/documents/580/download?locale=es (accessed on 15 February 2022).
49. Gesteira, L.G.; Uche, J.; de Oliveira Rodrigues, L.K. Residential Sector Energy Demand Estimation for a Single-Family Dwelling: Dynamic Simulation and Energy Analysis. *J. Sustain. Dev. Energy Water Environ. Syst.* **2021**, *9*, 1–18. [CrossRef]